Physics of the Earth and Planetary Interiors 230 (2014) 1–14

Contents lists available at ScienceDirect

Physics of the Earth and Planetary Interiors

journal homepage: www.elsevier.com/locate/pepi

Crust and upper mantle structure of the New Madrid Seismic Zone: Insight into intraplate earthquakes

Chuanxu Chen [a,b,c,*], Dapeng Zhao [a,*], Shiguo Wu [b]

[a] Department of Geophysics, Tohoku University, Sendai 980-8578, Japan
[b] Institute of Oceanography, Chinese Academy of Science, Qingdao, China
[c] University of Chinese Academy of Sciences, Beijing, China

ARTICLE INFO

Article history:
Received 18 July 2013
Accepted 23 January 2014
Available online 18 February 2014
Edited by Vernon F. Cormier

Keywords:
New Madrid Seismic Zone
Seismic tomography
Low-velocity zone
Intraplate earthquakes
Farallon slab
Seismotectonics

ABSTRACT

We determine a 3-D P-wave velocity model of the crust and upper mantle down to 400 km depth to investigate structural heterogeneity and its influences on the generation of intraplate earthquakes in the New Madrid Seismic Zone. We used 4871 high-quality arrival times from 187 local earthquakes and 30,846 precise travel-time residuals from 1041 teleseismic events recorded by the EarthScope/USArray Transportable Array. Our results show that, beneath the Reelfoot rift, a significant low-velocity (low-V) zone exists in the upper mantle down to 200 km depth, with a large volume of 200 × 200 × 150 km^3. The origin of the low-V zone may be related to the passage of the Bermuda hotspot and the stalled ancient Farallon slab materials foundering in the mantle transition zone. This low-V zone may have relatively low shear strength and act as a viscously weak zone embedded in the lithosphere, being apt to concentrate tectonic stress and transfer stress to the seismogenic faults in the upper crust, leading to the large intraplate earthquakes in the New Madrid Seismic Zone.

1. Introduction

The New Madrid Seismic Zone (NMSZ) is seismically the most active region in the Central and Eastern United States and an ideal area to study intraplate earthquakes. A sequence of at least three large earthquakes (M ⩾ 7.0) occurred here in 1811–1812 (e.g., Hough et al., 2003; Johnston and Schweig, 1996), and palaeo-seismic records show evidence of large earthquakes about 500 years apart in the past 2000 years (e.g., Kelson et al., 1996; Tuttle et al., 2002). The distribution of local earthquakes recorded since 1974 delineates three linear faults in the NMSZ (see Fig. 1): (1) the NE-trending Cottonwood Grove-Blytheville Arch fault along the central Reelfoot rift, (2) the NW-trending Reelfoot Fault, and (3) the NNE-trending New Madrid North Fault (Johnston and Schweig, 1996). The activation of these mid-continental faults and their controls on duration of the seismic activity remain poorly understood. One of the fundamental questions is: what makes the NMSZ different from the surrounding intraplate areas in North America, especially the areas within the same geologic settings?

Several models have been proposed to explain the New Madrid seismic activity, such as a sinking mafic body in a reactivated lower crust (Pollitz et al., 2001), relaxation of a weak zone within an elastic lithosphere (Kenner and Segall, 2000; Liu and Zoback, 1997), unloading from deglaciation (Wu and Johnston, 2000) or river incision (Calais et al., 2010), and a localized mantle flow induced by deep mantle dynamics (Forte et al., 2007). In this work, we mainly test the model of a weak zone within the elastic lithosphere, because such a weak zone may exhibit seismic-velocity anomalies that may be detected by seismic tomography. This model postulates a weak zone within the lower crust and upper mantle, and the intraplate earthquakes are caused by stress transferred to the seismogenic faults from the mechanically weak zone (Kenner and Segall, 2000). However, there has been no clear evidence for such a weak zone and no obvious mechanism for the weakening (e.g., Calais et al., 2010) shown in the previous studies.

In this work we present a high-resolution three-dimensional (3-D) P-wave velocity model of both the crust and upper mantle under the NMSZ and its surrounding areas using a new and high-quality data set of both local earthquakes and teleseismic events recorded by the USArray. The present results shed new light on the crustal and upper-mantle structure and mechanism of the intraplate earthquakes in the NMSZ.

* Corresponding authors. Address: Department of Geophysics, Tohoku University, Sendai 980-8578, Japan. Tel.: +81 22 225 1950; fax: +81 22 264 3292 (C. Chen).
E-mail addresses: chencxiocas@gmail.com (C. Chen), zhao@aob.gp.tohoku.ac.jp (D. Zhao).

http://dx.doi.org/10.1016/j.pepi.2014.01.016
0031-9201/

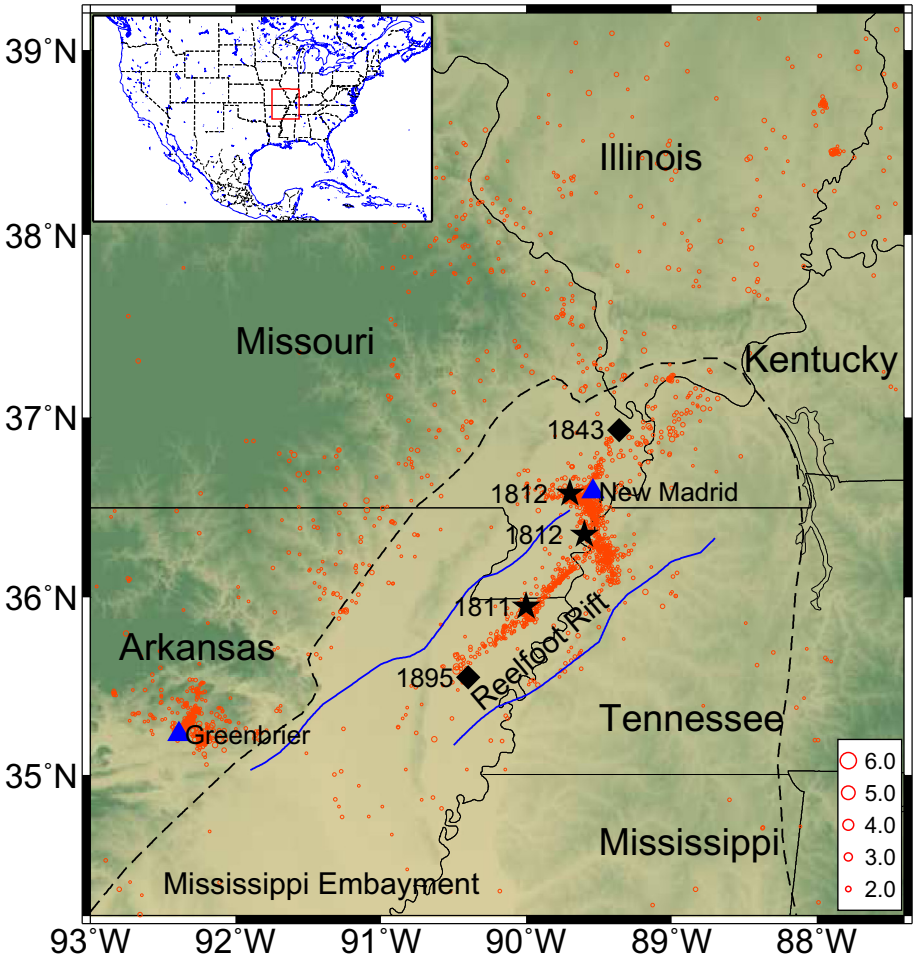

Fig. 1. Seismicity in the New Madrid Seismic Zone and adjacent areas. The red circles show the earthquakes compiled by the Center for Earthquake Research and Information catalogues from April 1974 to December 2012. The three black stars show the estimated epicenters of the large earthquakes (Mw $\geqslant$ 7.0) which occurred in 1811 to 1812 (Johnston and Schweig, 1996; Hough et al., 2003). The two diamonds show the estimated epicenters of the 1843 Marked Tree earthquake (M ~6.3) and the 1895 Charleston earthquake (M ~6.6). The black dashed line shows the estimated boundary of the Mississippi embayment, and the two blue lines delimit the Palaeozoic Reelfoot rift. The blue triangle shows the town New Madrid and Greenbrier. The inset map shows the location of the present study area (red box). Note that the cluster of seismicity near Greenbrier was associated with 2 earthquake swarms in 1981 and 2001 and recent seismicity was associated with waste water injection wells from hydrofrac operations in the gas fields there. (For interpretation of the references to color in this figure legend, the reader is referred to the web version of this article.)

2. Data and method

Two sets of seismic data are used to conduct tomographic inversions. One data set consists of arrival times from local earthquakes which occurred in and around the NMSZ (Fig. 2). The other is relative travel-time residuals from teleseismic events (Fig. 3). We used the first P-wave arrival times of both local and teleseismic events, which were collected precisely by the staff of the USArray Network Facility, and the recording period was from November 2010 to October 2012. During this period 63 seismic stations were densely and uniformly distributed in the study area (34.2–39.2°N, 87.4–93.0°W), and the station spacing is about 50 km (Fig. 2).

We selected the local earthquakes carefully based on the following criteria: (1) only events occurring during the local night time (02:00–12:00 UTC) were selected in order to exclude local quarry blasts which were conducted only in daytime; (2) each event was recorded by over 6 seismic stations; (3) the event magnitude (Mb) is $\geqslant$1.5; (4) before conducting tomographic inversion we relocated these local events using the Geiger method (Geiger, 1912; Zhao et al., 1992) and selected the events with uncertainties of <2 km in epicentral location and <8 km in focal depth. As a result, our data set contains 2500 first P-wave and 2371 S-wave arrival times from 187 local earthquakes (Fig. 2).

We also collected 1041 teleseismic events with magnitudes $M \geqslant 4.5$. Each event has at least 10 recordings, and the average number of data per event is up to 30. The distances between the teleseismic events and the center of the study area are restricted to 30–100° (Fig. 3), in order to avoid influences of the complex structures at the bottom of the mantle and those in the upper mantle outside the present study region (Zhao et al., 1994, 2013). The azimuthal coverage of the teleseismic events is fairly complete (Fig. 3). In total, we used 31,846 P-wave arrival times from the 1041 teleseismic events selected.

Relative travel-time residuals of the teleseismic events are computed and used in the tomographic inversion in order to avoid the effects of the complex structures in the crust and upper mantle under the hypocenters of every teleseismic events (Zhao et al., 1994). We first compute raw travel-time residuals by subtracting the theoretical travel times from the observed ones, and the 1-D iasp91 Earth model (Kennett and Engdahl, 1991) is adopted to calculate the theoretical travel times. Then we calculate the mean residual for each event averaged over all the recording stations. Finally, rel-